Datadriven HOPGD based computational vademecum for welding parameter identification

Ye Lu, Nawfal Blal, Anthony Gravouil

Datadriven HOPGD based computational vademecum for welding parameter identification

Y. Lu[1,2] · N. Blal[1] · A. Gravouil[1]

The paper presents a datadriven framework for parameter identification of welding models. Common identification procedures are based on iterative optimization algorithms which minimize the distance between experimental measures and simulations. The cost of repetitive evaluations of objective functions is prohibitive, especially in welding cases, due to the multiphysics, nonlinear and multiparametric aspects. This is why one proposes to use a novel datadriven approach to improve the efficiency of the inverse identification procedures. Based on a sparse sampling strategy, an a posteriori non-intrusive reduction method, i.e. HOPGD, is used in the offline training stage for constructing the *computational vademecum*. An online subspace learning method coupled with a global optimization algorithm is proposed for the online search. The efficiency of the proposed method for multiple parameters identification is demonstrated through examples based on a 3D welding model.

Keywords HOPGD · Datadriven · Parameter identification · *Computational vademecum* · Sparse sampling

1 Introduction

Identification of parameters for numerical models relies on an iterative opitmization procedure in which a large number of numerical simulations are required. Despite of the significant increasing of computer power, this inverse problem can still be extremely expensive in terms of CPU time, especially when encountering multiparameters cases (like welding) in which the response surfaces of objective functions may possess many local minima. In addition, welding simulations are usually costly due to the multiphysics, nonlinear and temporal aspects (see e.g. [3,37,43]).

One efficient way to accelerate the identification procedure is to use model order reduction methods. A posteriori projection-based reduction methods (e.g. Proper Orthogonal Decomposition (POD) [18,22,38], Principal Component Analysis [19], reduced basis methods [31,41]), consist in an offline training procedure which extracts reduced bases (RBs) from data (called snapshots) precomputed with standard finite element (FE) methods, and an online stage in which numerical solutions are projected on those RBs to construct efficient reduced order models. The main drawbacks of these approaches are the necessity of snapshots and the loss of efficiency with nonlinearities, although some online RB adaptation methods [2,42,45,46] and acceleration techniques [4,9] dealing with nonlinearities have been proposed. A priori methods, i.e. Proper Generalised Decomposition (PGD) [1,10,12], can eliminate the necessity of snapshots in the training stage. RBs are built on-the-fly once for all by solving the weak formulation of the problem. The resulting *computational vademecum* (formed by the RBs) [16,39,44] contains all possible solutions in the parameter space of interest and can therefore provide real-time responses in the online stage. This kind of approaches has enabled efficient inverse identification in dynamic datadriven application systems [14,17]. However, the intrusiveness of these methods makes their implementation in an existing commercial code very difficult. Furthermore, their application to nonlinear dissipative processes is not straightforward, although PGD based approaches have been successfully applied to transient thermal analysis for welding [8]. Hyper-reduction method [42,45,46] seems more successful in welding prob-

✉ A. Gravouil
Anthony.Gravouil@insa-lyon.fr

Y. Lu
Ye.Lu@insa-lyon.fr

N. Blal
Nawfal.Blal@insa-lyon.fr

[1] Univ Lyon, INSA-Lyon, CNRS UMR5259, LaMCoS, 69621 Villeurbanne, France

[2] Chaire AREVA-SAFRAN, INSA, Lyon, France

lems. However, the intrusiveness and the necessity of online computational effort restrict its widely use. A posteriori non-intrusive reduction methods [6,28–30] can fully overcome these difficulties. These methods are mainly based on the offline database construction and interpolation techniques that prevent online full computations. Very recently, a series of non-intrusive methods [28–30] as well as efficient sampling strategies in high dimensional spaces have been proposed and applied in welding simulations. The employment of the temporal aspect of problems in these methods allows to overcome the nonlinearity difficulties associated with the projection-based reduction methods and leads to space-time *computational vademecum* that can provide real-time online simulations. These results encourage one to define a datadriven framework for efficient inverse identification.

Datadriven engineering has received a constantly increasing attention as the progress of machine learning, big data, data mining techniques in computer science over the last decades. In the context of computational engineering, [23] proposed a datadriven computing framework in which material constitutive models are replaced by pure experimental data. Although the collection of experimental data remains an open question, this method opens numerous appealing perspectives in computational mechanics, since the hypothesis of material models, which is usually the main inaccuracy resource in standard FE computations, can be totally avoided. The same idea has been applied to material response characterization [27], computational elasticity and inelasticity [20,21], dynamic problems [24]. Many other researches attempted to applied machine learning techniques in material discovery, design and modeling across different scales with experimental or simulation data (see e.g. [5,36,40]). For the identification of material parameters, [33] proposed to use a reduced shape manifold learning approach within the framework of an indentation test. This method is based on POD and a predictor-corrector local data enrichment strategy. However, as mentioned in [34], this method converges still slowly and usually leads to a local minimum (which is not necessarily the global optimal solution). In high dimensional cases, this can be a restriction for the use of the method.

The objective of this work is to propose an offline-online datadriven framework for efficient identification of parameters in welding. The presented cases are based on a 3D welding model. The snapshots are generated using a commercial code (i.e. ABAQUS). A non-intrusive reduction method, i.e. Higher Order PGD (HOPGD) [28,35], together with an adaptive sparse sampling strategy [28], is used in the offline training stage for their efficiency in high dimensional cases. In order to avoid the local minimum problem and the redundancy of data, an online subspace learning strategy coupled with a global optimization method is proposed. As a first attempt, the application examples are considered in a deterministic framework, in which the noise and uncertainties of measurement are not taken into account. The efficiency of the proposed method will be shown through examples of 2 and 3 parameters.

To achieve this goal, this paper is organized as follows. Section 2 introduces the concerned thermomechanical formulation and a FE model of welding. Then, the offline HOPGD based training strategy for constructing the *computational vademecum* is presented in Sect. 3. Section 4 will present the online search algorithms for the inverse identification, in which a global optimization and a subspace learning strategy are proposed. Finally, Sect. 5 will give two identification examples using the proposed approach.

2 Problem statement

2.1 Thermomechanical formulation

Let us consider a transient thermo-elasto-plastic problem with a moving heat source. This case is usually considered in a macroscopic modeling of welding. Under weak coupling assumption, the transient heat transfer analysis can be carried out prior to the mechanical analysis, by solving the following governing equation with boundary conditions (BCs)

$$\begin{cases} \rho C \dfrac{d\theta(\mathbf{X},t)}{dt} + \text{div}\ \mathbf{q}(\mathbf{X},t) = r(\mathbf{X},t) \quad \text{in the material domain } \Omega, \\ \mathbf{q}(\mathbf{X},t)\cdot\mathbf{n}(\mathbf{X},t) = \overline{\text{q}}(\mathbf{X},t) \quad \text{on the surface } \partial_{\mathbf{q}}\Omega, \\ \theta(\mathbf{X},t) = \overline{\theta}(\mathbf{X},t) \quad \text{on the surface } \partial_{\theta}\Omega, \\ \theta(\mathbf{X},t=0) = 0, \end{cases} \tag{1}$$

where θ is the variation of temperature with respect to initial state $\theta = T - T_0$, $\mathbf{q}$ is the heat flux vector, "div $\bullet$" is the divergence operator with respect to the initial position $\mathbf{X}$, d$\bullet$/dt the material time derivative, ρ and C are respectively the material density and specific heat capacity, and r is the internal heat generation. The Fourier constitutive law relates the heat flux to the temperature gradient

$$\mathbf{q}(\mathbf{X},t) = -\mathbf{k}\cdot\nabla\theta(\mathbf{X},t), \tag{2}$$

where $\mathbf{k}$ is the thermal conductivity. In isotropic cases, $\mathbf{k}$ can be simplified to a scalar k.

Generally, the boundary condition on $\partial_{\mathbf{q}}\Omega$ is enforced as a function of temperature. For instance, in the case of convection, $\overline{\text{q}} = h(T_{ext} - T) = h(T_{ext} - \theta - T_0)$, where T_{ext} denotes the external ambiance temperature, h denotes the heat transfer coefficient on the interface.

Mechanical analysis consists in seeking the admissible fields $\boldsymbol{\sigma}$, $\mathbf{u}$ and $\boldsymbol{\varepsilon}_p$ satisfying the following balance equations and BCs

$$\begin{cases} \text{div}\,\boldsymbol{\sigma}(\mathbf{X},t) = 0 \quad \text{in } \Omega, \\ \boldsymbol{\sigma}(\mathbf{X},t)\cdot\mathbf{n}(\mathbf{X},t) = \overline{\mathbf{F}}(\mathbf{X},t) \quad \text{on } \partial_{\mathbf{F}}\Omega, \\ \mathbf{u}(\mathbf{X},t) = \overline{\mathbf{u}}(\mathbf{X},t) \quad \text{on } \partial_{\mathbf{u}}\Omega, \end{cases} \tag{3}$$

where the body forces are neglected, $\boldsymbol{\sigma} = \mathbf{D} : \boldsymbol{\varepsilon}_e = \mathbf{D} : (\boldsymbol{\varepsilon} - \boldsymbol{\varepsilon}_p - \boldsymbol{\varepsilon}_\theta)$ with $\boldsymbol{\varepsilon} = \nabla_s \mathbf{u}(\mathbf{X},t)$, under infinitesimal strain assumption, and $\mathbf{D}$ denotes the fourth order elasticity tensor. The thermal strain denoted by $\boldsymbol{\varepsilon}_\theta$ results from the thermal expansion: $\boldsymbol{\varepsilon}_\theta = \alpha\theta\mathbf{I}$, where $\mathbf{I}$ is the second-order identity tensor and α is the thermal expansion coefficient. The complementary plastic behavior law with an isotropic hardening R reads

$$\begin{cases} f(\boldsymbol{\sigma}, \mathrm{p}) = \parallel \boldsymbol{\sigma}_d \parallel - \sigma_y - \mathrm{R}(\mathrm{p}), \\ \dot{\boldsymbol{\varepsilon}}_p = \mathcal{H}(f)\dfrac{< \boldsymbol{\sigma}_d : \dot{\boldsymbol{\sigma}}_d >}{\mathrm{R}g}\dfrac{\boldsymbol{\sigma}_d}{\parallel \boldsymbol{\sigma}_d \parallel}, \end{cases} \tag{4}$$

where σ_y denotes the initial yield stress, $\mathcal{H}(\bullet)$ the Heaviside function, $\boldsymbol{\sigma}_d$ the deviatoric stress tensor, $< A >$ the positive part of A, and p the equivalent plastic strains and $g = \frac{d\mathrm{R}}{d\mathrm{p}}$.

Weak formulations equivalent to (1) and (3) can be written, respectively, with test functions θ^* and $\mathbf{u}^*$

$$\int_\Omega \rho C\dot{\theta}\theta^* d\Omega + \int_\Omega \nabla\theta\cdot\mathbf{k}\cdot\nabla\theta^* d\Omega + \int_{\partial_{\mathbf{q}}\Omega} \bar{\mathrm{q}}\theta^* ds = \int_\Omega r\theta^* d\Omega. \tag{5}$$

and

$$-\int_\Omega \boldsymbol{\sigma}(\mathbf{u}) : \boldsymbol{\varepsilon}(\mathbf{u}^*) d\Omega + \int_{\partial_{\mathbf{F}}\Omega} \bar{\mathbf{F}}\cdot\mathbf{u}^* ds = 0. \tag{6}$$

This problem can be discretized by FE method and solved by a first order integrator and a nonlinear solver (e.g. Newton-Raphson), which consists in solving, at each time step k, the transient thermal problem

$$\mathbf{C}\dot{\boldsymbol{\theta}}(t_k) + \mathbf{K}\boldsymbol{\theta}(t_k) = \mathbf{Q}(t_k), \tag{7}$$

where

$$\begin{aligned} \mathbf{C} &= \int_\Omega \mathbf{N}^T \rho C \mathbf{N}\, d\Omega, \\ \mathbf{K} &= \int_\Omega \mathbf{B}^T \mathbf{k}\mathbf{B}\, d\Omega, \\ \mathbf{Q} &= \int_{\partial_{\mathbf{q}}\Omega} \mathbf{N}^T \bar{\mathbf{q}}\, ds + \int_\Omega \mathbf{N}^T r\, d\Omega. \end{aligned} \tag{8}$$

or in nonlinear cases where the properties of materials (e.g. ρ, C, $\mathbf{k}$) are temperature-dependent

$$\mathbf{C}(\theta)\dot{\boldsymbol{\theta}}(t_k) + \mathbf{K}(\theta)\boldsymbol{\theta}(t_k) = \mathbf{Q}(t_k). \tag{9}$$

and the quasi-static mechanical problem

$$\mathbf{F}_{int}(t_k) = \mathbf{F}_{ext}(t_k), \tag{10}$$

where

$$\begin{aligned} \mathbf{F}_{ext}(t) &= \int_{\partial_{\mathbf{F}}\Omega} \mathbf{N}^T \bar{\mathbf{F}}\, ds, \\ \mathbf{F}_{int}(t) &= \int_\Omega \mathbf{B}^T \boldsymbol{\sigma}\, d\Omega, \end{aligned} \tag{11}$$

with the shape function and its gradient denoted by $\mathbf{N}$ and $\mathbf{B}$ respectively.

2.2 Welding FE model

This section presents a macroscopic FE model of welding which consists in studying the history of thermomechanical loading of process in order to determine the distortions or residual stresses. Figure 1 illustrates an example of T-joints: two plates of width 3.2 mm are welded with approximately 90° to each other at the joint.

As suggested by [15], a double ellipsoidal model is used to describe the thermal heat source

$$\begin{cases} r(x,y,z) = \dfrac{6\sqrt{3}Qf_i}{abc_i\pi\sqrt{\pi}}\exp\left[-\left(\dfrac{x^2}{c_i^2}+\dfrac{y^2}{a^2}+\dfrac{z^2}{b^2}\right)\right], \quad i = 1, 2 \\ f_1 + f_2 = 2, \end{cases} \tag{12}$$

where Q is the effective welding heat input, x, y and z are the local coordinates of the double ellipsoid model in a moving frame attached to the weld torch, as shown in Fig. 2. a, b and c_i are the radial distances from the center of the heat source respectively in the lateral, vertical and axial directions. $i = 1$ or 2 denotes the ellipsoidal region before or after the

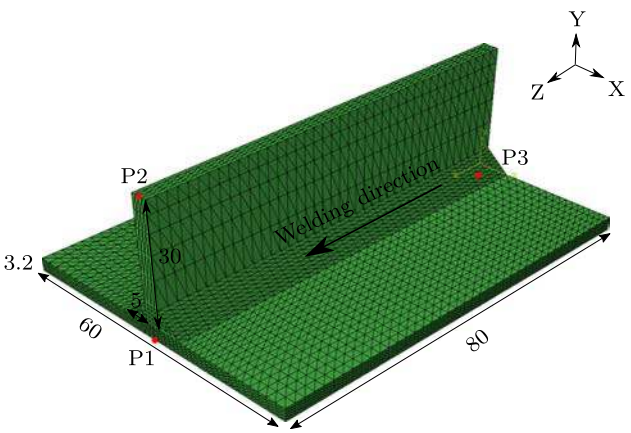

Fig. 1 FE model of T joint—single pass weld (units: mm)

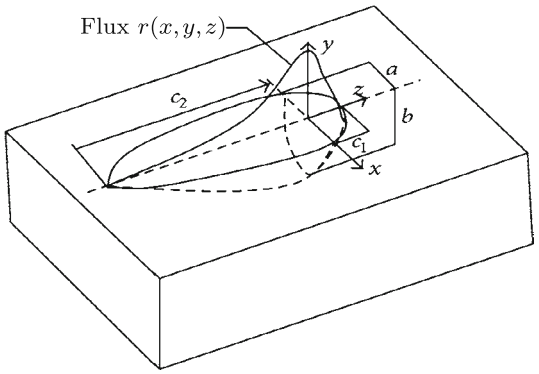

Fig. 2 Double ellipsoid model of heat source [15]

Table 1 Parameters of heat source

Q	a	b	c_1	c_2	Velocity
2680.35 W mm^{-3}	7.5 mm	7.5 mm	7.5 mm	30 mm	6.35 mm s^{-1}

torch passes. f_i are the heat input fractions. Table 1 shows the parameters used in this work. In addition, $f_1 = 0.6$ and therefore $f_2 = 1.4$, as suggested by [15], which were found to provide a good agreement with experimental thermal history results.

The material properties of stainless stell AL-6XN are used and considered temperature-dependent in the thermo-mechanical analysis (see e.g. Fig. 3). The isotropic hardening coefficient is assumed constant at any temperature. Boundary conditions for both thermal and mechanical aspects are shown in Table 2. The material properties and boundary conditions are taken to be the same as in [43].

This model is discretized using linear tetrahedral elements, with 4 elements across the thickness (Fig. 1). The mesh is refined for those regions close to the heat source. This yelds in total 29,571 elements and 7299 nodes. The thermal and mechanical problems are assumed weakly coupled and solved alternatively at each incremental time step. Note that a fully coupled solution strategy can also be applied, and this will not change fundamentally the proposed identification framework. Figure 4 depicts an example of FE analysis with parameters used in [43]. In practice, these parameters, including those of thermal source and materials, should be identified in comparison of experimental measures of quantities of interest (temperature, residual stresses or distortions).

Considering an inverse identification problem

$$\begin{cases} \text{Find} \quad \boldsymbol{\mu} \in \mathcal{D} \quad \text{s.t.} \\ \boldsymbol{\mu} = \underset{\boldsymbol{\mu}^* \in \mathcal{D}}{\arg\min}\, J\left(\mathbf{u}, \mathbf{u}^e, \boldsymbol{\mu}^*\right), \end{cases} \tag{13}$$

where $\boldsymbol{\mu} = [\mu_1, \mu_2, \ldots, \mu_d]^T$ is a vector containing the material and loading parameters to be identified, $\mathcal{D}$ is the multidimensional parameter space (design space) which is supposed large enough for identification. The objective function $J : \Omega_x \times \Omega_t \to \mathbb{R}$ depending on the quantity of interest $\mathbf{u}$ and parameters $\boldsymbol{\mu}^*$ is usually defined as a relative error with respect to some (experimental) references $\mathbf{u}^e$. To solve this problem, standard approaches use an optimization algorithm and recall numerous times the FE model for computing $\mathbf{u}$. This is a time-costly procedure for welding due to its transient and nonlinear aspects. Although analytic formula can be introduced for sensitivity analysis in some cases so as to alleviate the computational cost [43], the implementation complexity and the cost of sensitivity analysis itself remain a heavy burden.

In what follows, a novel datadriven framework is presented for efficient identification of welding model parameters.

3 Offline training strategy for building the space-time multiparametric *computational vademecum*

This section presents a non-intrusive reduction method, i.e. HOPGD [28,29,35], for constructing *computational vademecum* in the parameter space. The training snapshots can be computed by any available commercial code.

3.1 Sparse grid based HOPGD

Similarly to higher-order SVD or PARAFAC methods [25], the HOPGD can be used to obtain separated approximations of known functions. Given a d-dimensional scalar-valued function $f(\mu_1, \mu_2, ..., \mu_d)$ with coordinates $\mu_i|_{i=1,d} \in \mathcal{D}_i$ and $\mathcal{D} = \mathcal{D}_1 \times \mathcal{D}_2 \times \cdots \times \mathcal{D}_d$, the HOPGD seeks a L^2 projection of the original known function in the following form

$$\begin{aligned} f(\mu_1, \mu_2, ..., \mu_d) &\approx f^n(\mu_1, \mu_2, ..., \mu_d) \\ &= \sum_{m=1}^{n} F_1^m(\mu_1) F_2^m(\mu_2) \cdots F_d^m(\mu_d), \end{aligned} \tag{14}$$

where f^n is an approximation of f and n is the rank of approximation. The n-rank approximation f^n is given by the finite sum of products of the separated functions: $F_i^m|_{i=1,d}$, which are a priori unknown and should be obtained by the L^2 projection. Furthermore, each function F_i^m that represents a variation of the original function f in the parameter direction μ_i is also called a mode function. For computational purposes, the approximation can also be written in the following incremental form by considering that the f^{n-1} is already computed previously

$$f^n(\mu_1, \mu_2, ..., \mu_d) = f^{n-1} + F_1^n(\mu_1) F_2^n(\mu_2) \cdots F_d^n(\mu_d). \tag{15}$$

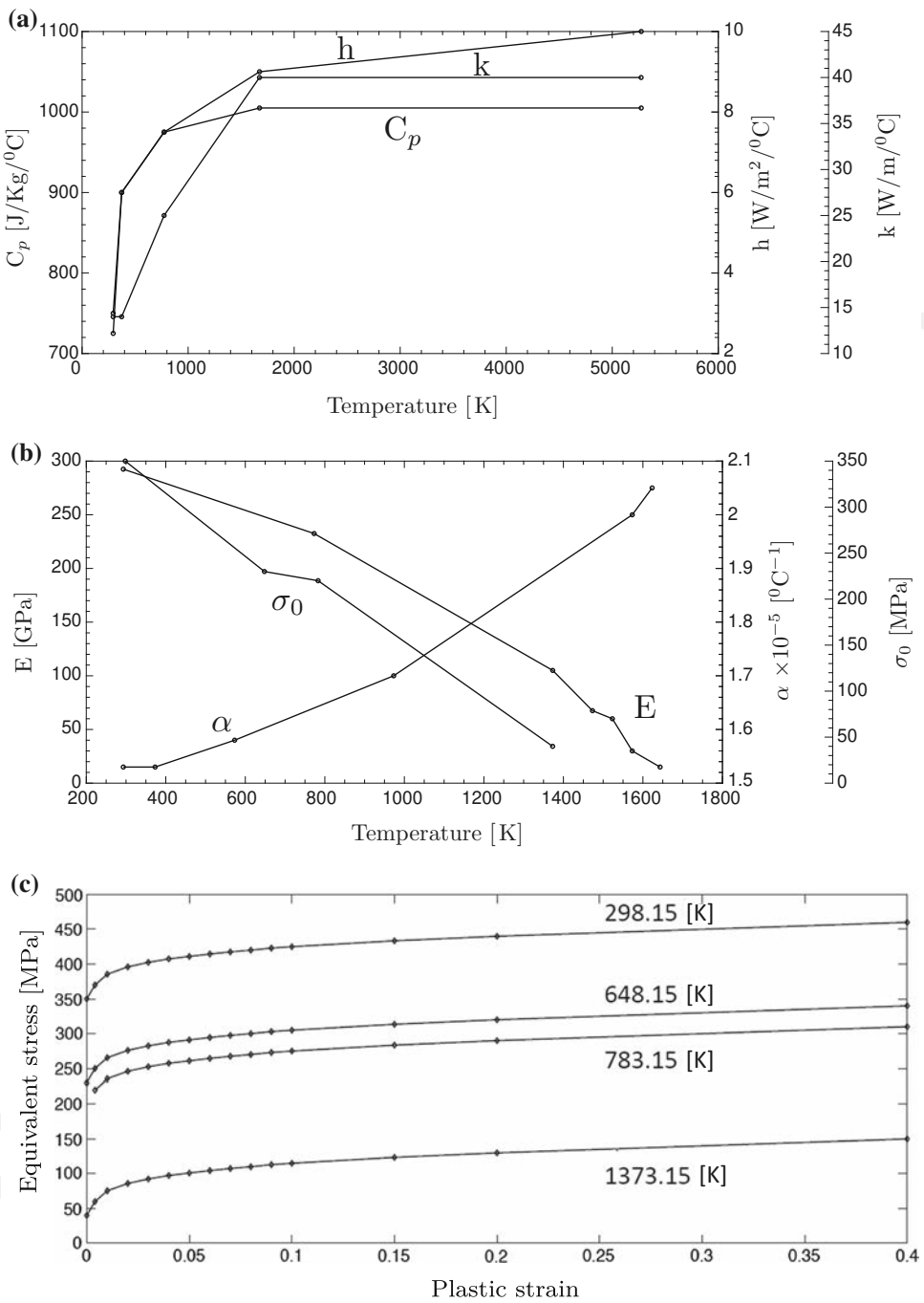

Fig. 3 Evolution of thermal and mechanical properties with temperature for AL-6XN [43]

The L^2 projection is formulated as a minimization problem as follows

$$\begin{cases} \text{Find } f^n \in V_n \subset L^2(\mathcal{D}) \text{ s.t.} \\ J(f^n) = \min_{f^n} \left(\frac{1}{2} \parallel f^n - f \parallel^2_{L^2(\mathcal{D})} \right), \end{cases} \tag{16}$$

or equivalently the solution of

$$(f^n, f^s)_{\mathcal{D}} = (f, f^s)_{\mathcal{D}} \quad \forall s \in [1, n], \tag{17}$$

where $f^s = \prod_{i=1}^{d} F_i^s$, and $(\bullet, \bullet)_{\mathcal{D}}$ denotes the integral of the scalar product over the domain $\mathcal{D}$. Thanks to the separation of variables, the left hand side integration over the d-dimensional domain are simple products of 1D integrals

$$(f^n, f^s)_{\mathcal{D}} = \sum_{m=1}^{n} \prod_{i=1}^{d} (F_i^m, F_i^s)_{\mathcal{D}_i}. \tag{18}$$

Different from PARAFAC method, HOPGD uses a greedy algorithm to compute the separated functions for f^n. At each

Table 2 Thermal and mechanical boundary conditions

Constrained point	Prescribed condition
Exposed surfaces	Convection
P1	Displacement constrained in X, Y, Z
P2	Displacement constrained in X
P3	Displacement constrained in X, Y

enrichment step n, the following local optimization problem is solved

$$\left(\prod_{i=1}^{d} F_i, \delta f\right)_{\mathcal{D}} = \left(f - f^{n-1}, \delta f\right)_{\mathcal{D}}, \tag{19}$$

with test functions $\delta f = \delta \prod_{i=1}^{d} F_i = \delta F_1 F_2 ... F_d + F_1 \delta F_2 ... F_d + \cdots + F_1 F_2 ... \delta F_d$. Thus, for a known function f and having estimated the $n-1$ rank of this function in a separated form f^{n-1}, the next step consists in the estimate of the other separated modes F_1, F_2, ..., F_d at the rank n using the above equation.

The definition of HOPGD in sparse cases [28] where the domain $\mathcal{D}$ is not fully sampled with a conventional structured grid can be written as

$$\begin{cases} \text{Find } f^n \in V_n \subset L^2(\mathcal{D}) \text{ s.t.} \\ J(f^n) = \min\limits_{f^n} \left(\frac{1}{2} \parallel wf^n - wf \parallel^2_{L^2(\mathcal{D})} \right), \end{cases} \tag{20}$$

where w is a sampling index equal to 1 or 0, depending on the sampling strategy in the parameter space $\mathcal{D}$. This means the

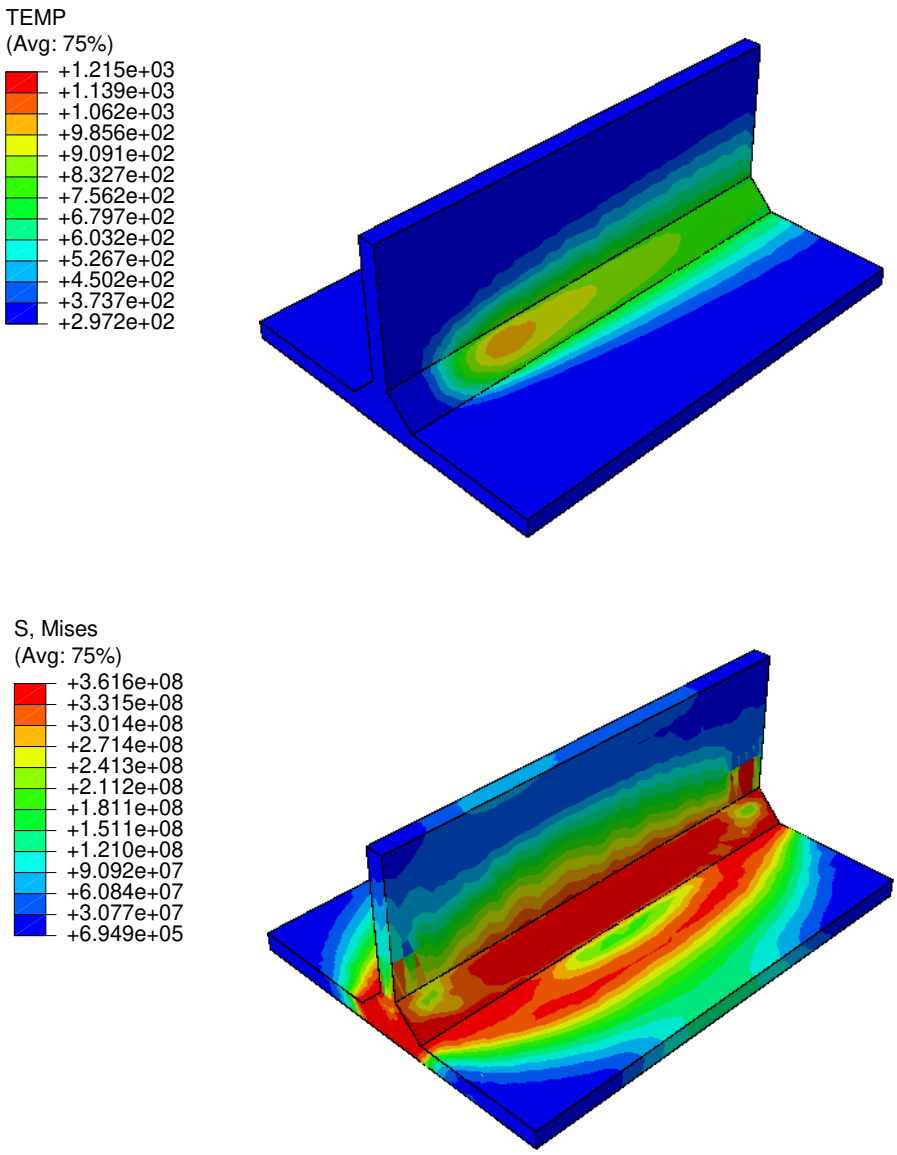

Fig. 4 FE simulation using parameters suggested by [43]. Top: temperature (K) at an intermediate time step corresponding to $t = 12$ s. Bottom: residual stresses (Pa) at final time $t = 60$ s

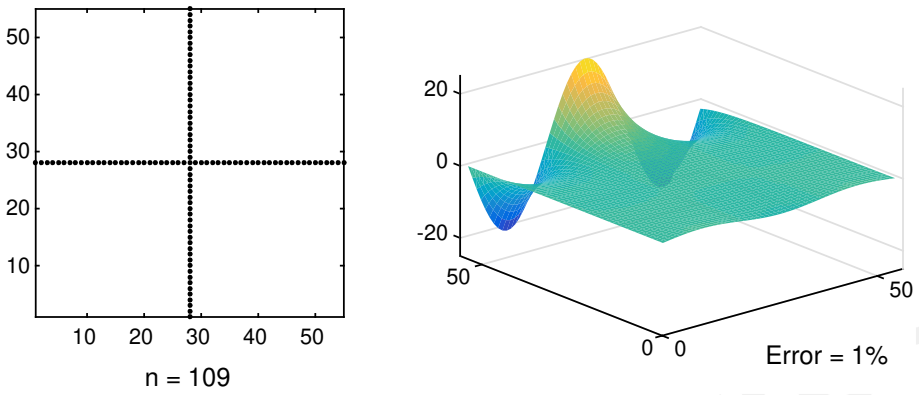

Fig. 5 Axes refinement (left) and corresponding approximated surface (right) for the separated function: $z(x, y) = \sin(\pi x)\frac{\sinh(\pi y)}{\sinh(\pi)}$

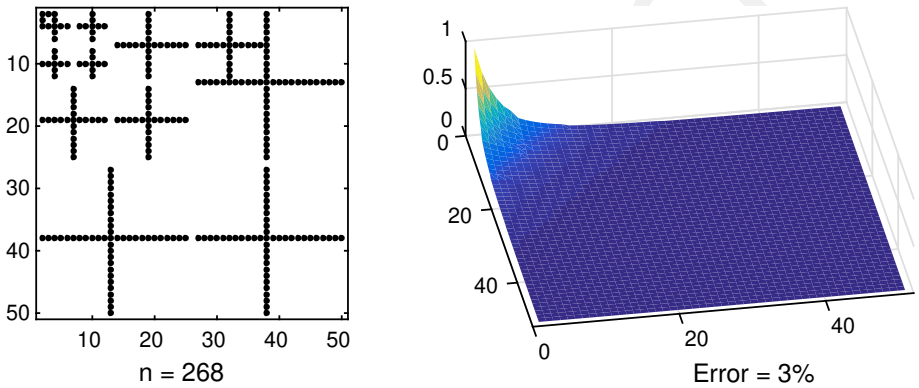

Fig. 6 Adaptive sparse grid sampling (left) and corresponding approximated surface (right) for the 'corner peak' function: $z(x, y) = (c_1 + c_2 x + c_3 y)^{-3}$

approximated function f^n minimizes only the error on sampling points. Considering the incremental form of equation (14), the solution at step n is given by solving the following local optimization problem

$$\left(w\prod_{i=1}^{d} F_i, \delta f\right)_{\mathcal{D}} = \left(wf - wf^{n-1}, \delta f\right)_{\mathcal{D}}. \tag{21}$$

An alternating fixed point algorithm is used to solve this problem. The implementation aspect can be found in [28]. It should be highlighted that the sparse sampling is the key point to overcome the exponentially increasing complexity of the right hand side integral in equation (21).

3.2 Adaptive sampling

The use of standard full grids for sampling multidimensional parameter space will encounter the well-known curse of dimensionality. In order to overcome this difficulty, an adaptive sparse sampling strategy [28] can be used. This is based on an a posteriori error indicator defined as the distance between the approximated and "exact" solutions (usually computed with high-fidelity models). Denoting by $\hat{u}$ a quantity of interest approximated by HOPGD, its distance from the exact solution u is measured by a L^2 norm

$$\mathrm{Err}(\hat{u}) = \frac{\| \hat{u} - u \|_{L^2}}{\| u \|_{L^2}}. \tag{22}$$

The idea is to sample the axes of those sub-domains in which the approximation precision provided by the aforementioned error indicator is not satisfied. The first level refinement in a 2D parameter space is performed along its two symmetric axes (see e.g. Fig. 5). The error of each generated sub-domain is computed by choosing an assessment point (e.g. the central point of sub-domain). Local refinements will be then successively performed until the global approximation error is lower than a given tolerance. Examples using sparse grid sampling and HOPGD to approximate different analytic functions are illustrated in Figs. 5, 6 and 7. It can be noticed that the number of samples (snapshots) depends on the separability of original functions and is significantly reduced comparing with full grids. Higher dimension (up to 6) examples can be found in [28]. As it is mentioned in [28], the error indicator requiring pre-computed "exact" solutions may be very expensive in those cases. This difficulty should be overcome, for instance, by considering a more complex residual based indicator. However, this is not at the heart of present work.

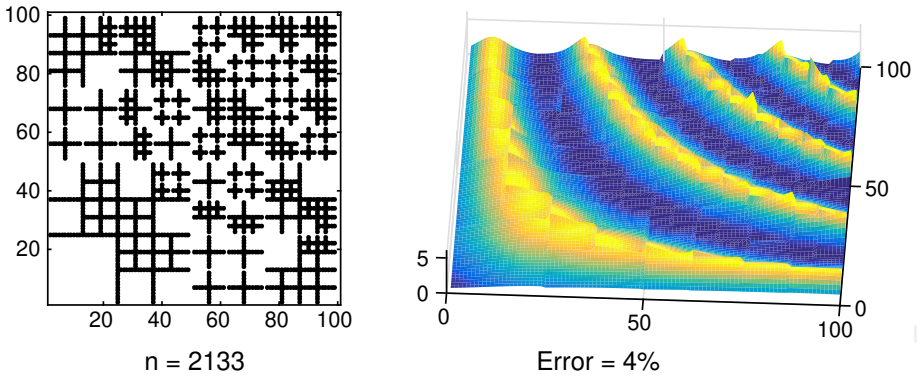

Fig. 7 Adaptive sparse grid sampling (left) and corresponding approximated surface (right) for the 'planar waves' function: $z(x, y) = e^{\sin(kxy)}$

3.3 Space-time computational vademecum for efficient identification

The aforementioned method has enabled a series of space-time *computational vademecum* [28,29]. It should be highlighted here that the temporal aspect of these *computational vademecum* is one of the most important features that differ from other POD or PGD based *vademecum* (e.g. [11,13]) built for optimization and design processes. The offline available space-time solutions are the key point for efficient online parametric studies of transient nonlinear problems like welding.

The *computational vademecum* is formed by the reduced bases of HOPGD and can provide real time online parametric solutions. Denoted by $\mathbf{u}^i(\mathbf{X}, t)$ snapshots computed for some combinations of parameter values $\boldsymbol{\mu}^i$ selected by the sparse grid strategy, they can be ranged in a $(4 + d)$-dimensional sparse matrix

$$\begin{cases} \mathbf{u}(\mathbf{X}, t, \boldsymbol{\mu}) = \mathbf{u}^i(\mathbf{X}, t) & \text{when } \boldsymbol{\mu} = \boldsymbol{\mu}^i, \\ \mathbf{u}(\mathbf{X}, t, \boldsymbol{\mu}) = 0 & \text{when } \boldsymbol{\mu} \neq \boldsymbol{\mu}^i. \end{cases} \tag{23}$$

HOPGD can then be employed to extract separated reduced bases from the above data matrix

$$\begin{cases} \hat{\mathbf{u}}(\mathbf{X}, t, \boldsymbol{\mu}) = \sum_{m=1}^{n} \boldsymbol{\Phi}^m(\mathbf{X}) \otimes \mathbf{V}^m(t) \otimes \boldsymbol{F}_1^m(\mu_1) \otimes \cdots \otimes \boldsymbol{F}_d^m(\mu_d), \\ \text{with} \quad \hat{\mathbf{u}}(\mathbf{X}, t, \boldsymbol{\mu}) \approx \mathbf{u}(\mathbf{X}, t, \boldsymbol{\mu}) \quad \text{when } \boldsymbol{\mu} = \boldsymbol{\mu}^i, \end{cases} \tag{24}$$

where functions $\boldsymbol{\Phi}$ and $\mathbf{V}$ are respectively the space and time bases. The parameter functions $\boldsymbol{F}_i$ are then the so-called parameter bases. It should be noticed that storing these reduced bases is much cheaper than storing the original data matrix. The separated representation involves therefore a reduced database (*computational vademecum*). For those parameters $\boldsymbol{\mu}^* = \boldsymbol{\mu}^i$, $\hat{\mathbf{u}}$ is an approximation of $\mathbf{u}^i$. For $\boldsymbol{\mu}^* \neq \boldsymbol{\mu}^i$, $\hat{\mathbf{u}}$ contains the prediction made by the reduced bases learned from $\mathbf{u}^i$. Furthermore, the prediction for unknown parameters $\boldsymbol{\mu} \neq \boldsymbol{\mu}^i$ is very fast, since only 1D interpolation is needed, i.e.

$$\hat{\mathbf{u}}(\mathbf{X}, t, \boldsymbol{\mu}^*) = \sum_{m=1}^{n} \boldsymbol{\Phi}^m(\mathbf{X}) \otimes \mathbf{V}^m(t) \otimes \boldsymbol{F}_1^m(\mu_1^*) \otimes \cdots \otimes \boldsymbol{F}_d^m(\mu_d^*), \tag{25}$$

with $\boldsymbol{F}_i^m(\mu_i^*) = \mathbf{N}^T(\mu_i^*)\boldsymbol{F}_i^m$, and $\mathbf{N}(\mu_i)$ is a 1D FE basis.

Once the *computational vademecum* is available, the online prediction for $\mathbf{u}$ in problem (13) becomes very cheap. Coupled with a gradient-based optimization algorithm, fast identification can be expected. A straightforward alternative is to apply direct search strategies [26] which do not rely on the computation of derivatives of objective function J. Regardless of the low convergence rates, direct strategies are frequently used in industry, since they are usually very easy to implement and derivatives of objective function are not accessible in many cases. The construction of *computational vademecum* is obviously advantageous for this kind of approaches.

In this work, one relies on gradient-based methods for the reason of efficiency. In order to reduce data redundancy, the *computational vademecum* is constructed offline for a prescribed relatively important error in the global domain of parameters. For the accuracy of identification, an online subspace learning strategy dedicated to enrich snapshots in limited sub-domains will be presented in next section.

One remarks that when the online identification is strictly constrained by real time requirement, the *computational vademecum* should be constructed offline once for all for a sufficient accuracy in the whole global domain. However, this is not the case in many situations. Furthermore, in the presented method, it can be expected that the *computational vademecum* will become more and more rich (accurate) with its online uses, the online stage for identification will be therefore more and more fast.

4 Online search algorithms for parameter identification

Gradient-based optimization algorithms like conjugate gradient method, sequential quadratic programming (SQP), usually converge to a local minimum and depend on the initial guess. However, the assumptions of convexity or unimodality of objective function J cannot be made in many cases.

Based on *computational vademecum*, this section presents a global optimization method incorporated with an online learning strategy, in order to find a global minimum for the identification problem.

4.1 Global optimization method

Standard global optimization algorithms, e.g. genetic algorithms, multistart, and simulated annealing, require that the function J is cheap to evaluate. When J is expensive, efficient algorithms [7] are needed. In this work, J can be rapidly evaluated by inquiring the *computational vademecum*, the standard algorithm, i.e. multistart, is chosen for its implementation simplicity.

4.1.1 Multistart algorithm

The idea of multistart [32] is to apply the local optimization algorithm from different initial points in order to discover the diversification of response surface and find the overall best output. Hence, multistart methods consist in two phases: the first one where the solution is generated by a local optimization method (e.g. conjugate gradient method), the second one where the solution is improved. A standard multistart method can be summarized in Algorithm 1.

Algorithm 1: Multistart procedure

Result: Global optimum
Input : Parameter space $\mathcal{D}$, objective function J
Output: The optimal solution $\boldsymbol{\mu}'$

Generation of initial points $\{\boldsymbol{\mu}_1, \ldots, \boldsymbol{\mu}_K\}$
for $k \leftarrow 1$ **to** K **do**
  $\boldsymbol{\mu}_0 \leftarrow \boldsymbol{\mu}_k$
  Apply a local optimization method with initial guess $\boldsymbol{\mu}_0$ to find $\boldsymbol{\mu}$
  if $J(\boldsymbol{\mu})$ improves the best **then**
    Update the best, $\boldsymbol{\mu}' \leftarrow \boldsymbol{\mu}$
  end
end
Return $\boldsymbol{\mu}'$

4.1.2 Sensitivity analysis

Local optimization methods need numerical derivatives of objective function. The separated representation of quantity of interest $\mathbf{u}$ (24) can give explicit forms of these derivatives

$$\frac{\partial J}{\partial \mu_i} = \left(\frac{\partial J}{\partial \mathbf{u}}\right)^T \frac{\partial \mathbf{u}}{\partial \mu_i}, \qquad i = 1, \ldots, d \tag{26}$$

with

$$\begin{cases} \dfrac{\partial \mathbf{u}}{\partial \mu_1} = \displaystyle\sum_{m=1}^{n} \boldsymbol{\Phi}^m \otimes \mathbf{V}^m \otimes \frac{\partial \boldsymbol{F}_1^m}{\partial \mu_1} \otimes \cdots \otimes \boldsymbol{F}_d^m, \\ \qquad\qquad \vdots \\ \dfrac{\partial \mathbf{u}}{\partial \mu_d} = \displaystyle\sum_{m=1}^{n} \boldsymbol{\Phi}^m \otimes \mathbf{V}^m \otimes \boldsymbol{F}_1^m \otimes \cdots \otimes \frac{\partial \boldsymbol{F}_d^m}{\partial \mu_d}. \end{cases} \tag{27}$$

The Hessian matrix can be given by

$$\begin{aligned} \frac{\partial^2 J}{\partial \mu_i \partial \mu_j} &= \left(\frac{\partial^2 J}{\partial \mathbf{u} \partial \mu_j}\right)^T \frac{\partial \mathbf{u}}{\partial \mu_i} + \left(\frac{\partial J}{\partial \mathbf{u}}\right)^T \frac{\partial^2 \mathbf{u}}{\partial \mu_i \partial \mu_j} \\ &= \left(\frac{\partial^2 J}{\partial^2 \mathbf{u}} \frac{\partial \mathbf{u}}{\partial \mu_j}\right)^T \frac{\partial \mathbf{u}}{\partial \mu_i} + \left(\frac{\partial J}{\partial \mathbf{u}}\right)^T \frac{\partial^2 \mathbf{u}}{\partial \mu_i \partial \mu_j}. \end{aligned} \tag{28}$$

Similarly, higher-order derivatives of objective function can be straightforwardly obtained by the derivatives of 1D parameter functions. Moreover, this can be done in real time.

4.2 Online subspace learning strategy

4.2.1 Error analysis

Denoted by E_{app} the approximation error of HOPGD for a given region of local minimum in the parameter space, E_{local} the distance from this local minimum to the global minimum, the residual E of a local optimum given by the multistart algorithm can be estimated by

$$E \leq E_{app} + E_{local} \tag{29}$$

Figure 8 illustrates an example of a local minimum obtained in the multistart procedure. It is easy to known that the residual of a local optimum should not be superior to the summation of the approximation error and the intrinsic local error. If the local minimum is a potential global optimal solution, which means $E_{local} \approx 0$, the corresponding residual should be additionally inferior to the approximation error, i.e. $E \leq E_{app} + E_{tol}$, where E_{tol} is a small tolerance for accounting errors from the measurement. In the ideal case, E_{tol} is set to 0.

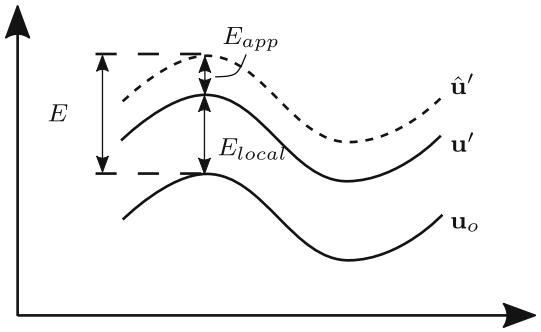

Fig. 8 Error analysis for a local minimum in multistart algorithms. $\mathbf{u}_o$: optimal solution (global minimum), $\mathbf{u}'$: solution at local minimum, $\hat{\mathbf{u}}'$: approximated solution using HOPGD at the local minimum

Hence, assuming a set of local minimum solutions $\{\boldsymbol{\mu}^{(k)}\}$ with their corresponding residual $\{E^{(k)}\}$ provided with the K starting points in Algorithm 1, one adopts following definitions:

- For $E^{(k)} \leq E^{(k)}_{app} + E_{tol}$, local minima $\boldsymbol{\mu}^{(k)}$ are referred to as admissible solutions (potential global minima).
- For $E^{(k)} > E^{(k)}_{app} + E_{tol}$, local minima $\boldsymbol{\mu}^{(k)}$ are referred to as non-admissible solutions.

In this work, the approximation error E_{app} is known with the error indicator computed for each sub-domain at current sampling grid. $E^{(k)}_{app}$ are related to those regions in which local minima appear. E_{tol} is set to 0, since the noise and uncertainties of experimental measures are not taken into account.

As mentioned earlier, *computational vademecum* is constructed for a relatively important error E_{app} at the offline stage. Local enrichment at the online stage will be needed to improve the precision of the subspaces that contain admissible solutions. This requires running the FE code for data construction and updating accordingly the *computational vademecum* with HOPGD. To this end, a subspace learning strategy is proposed hereafter for the selection of enrichment data points.

4.2.2 Subspace learning

The proposed subspace learning method consists in refining the sub-regions that potentially contain the global minimum. Denoted by $\mathcal{D}'$ the aforementioned regions containing admissible solutions, at each global iteration these domains $\mathcal{D}'$ are refined locally using sparse grids, as proposed by Sect. 3.

For the purpose of illustration, let us consider a 2D design space (see Fig. 9). Assuming that at iteration 0 (offline stage),

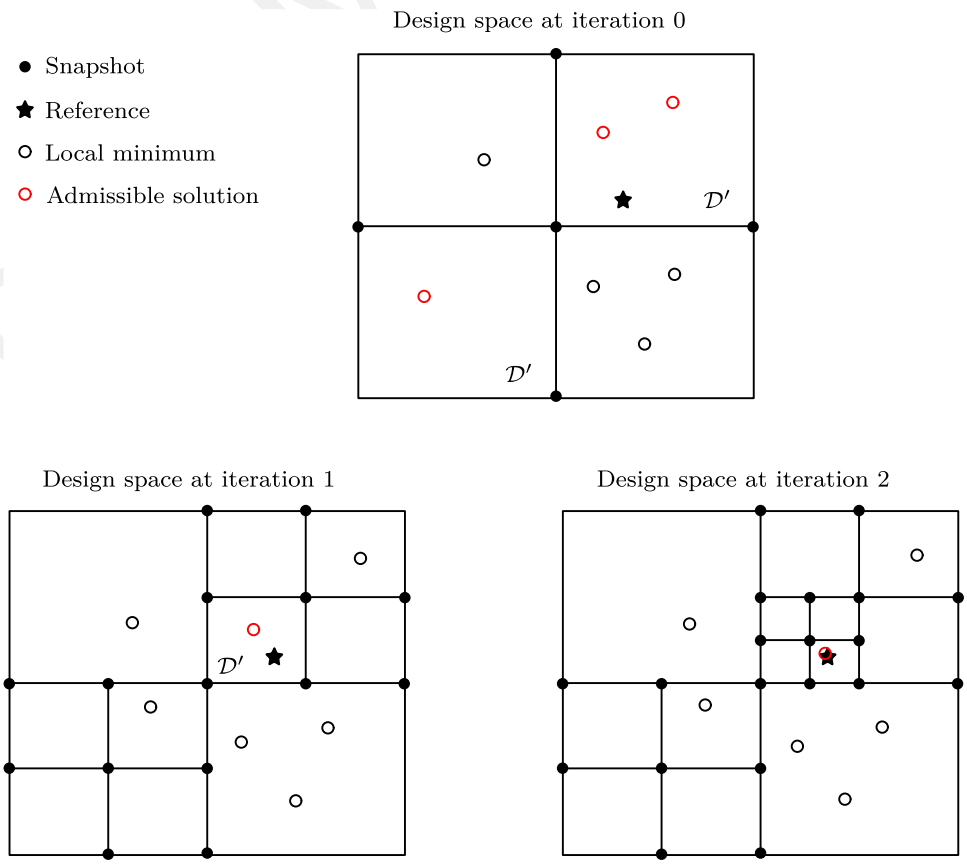

Fig. 9 Subspace learning in a 2D design space

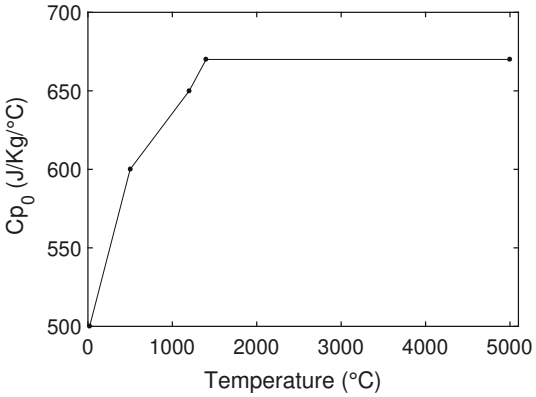

Fig. 10 Evolution of C_{p0} with temperature

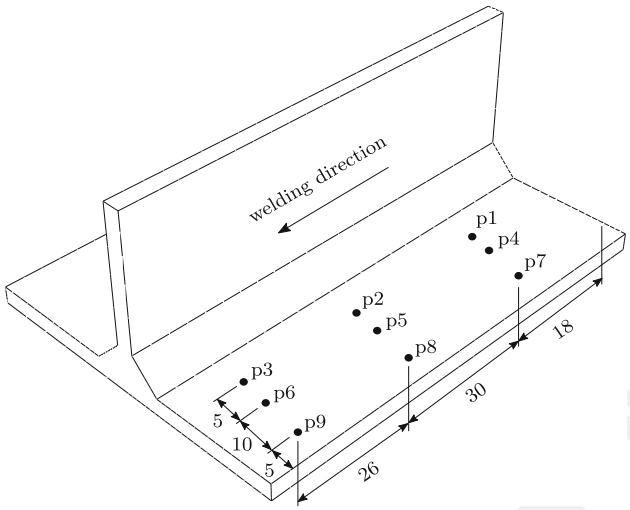

Fig. 11 Positions of thermocouples for temperature measurement

the global parameter space is already sampled by a sparse grid for a given level of accuracy and the *computational vademecum* is constructed with HOPGD. The multistart method with 7 randomly generated starting points gives then 7 local minima for the identification problem (13). The reference is considered as the optimal solution for the experimental measures of quantity of interest. As shown in Fig. 9, admissible solutions appear in two sub-domains $\mathcal{D}'$ at iteration 0 and they will be refined in next iteration. Multistart algorithm runs again in the global design space and finds new local minima. The admissible solutions approach to the reference as the learning procedure continues. The learning procedure is summarized in Algorithm 2.

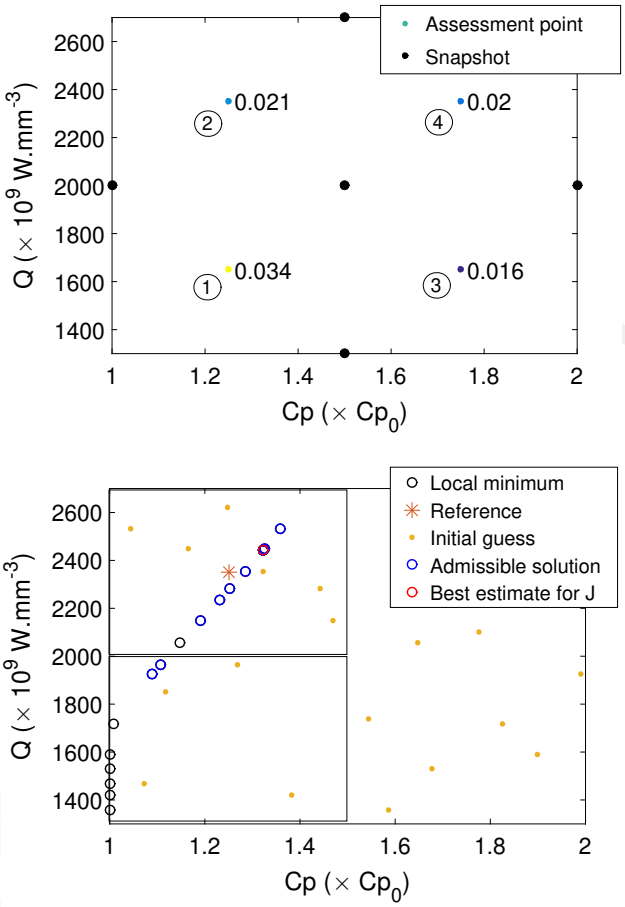

Fig. 12 Thermal parameter identification at iteration 0. Sampling grid with error assessment in design space (top) and multistart optimization (bottom)

Algorithm 2: Online subspace learning procedure

Result: Prediction for parameters
Input : Design space $\mathcal{D}$, offline *computational vademecum*
Output: The optimal solution $\boldsymbol{\mu}_{\text{opt}}$

Local minima and current global minimum $\boldsymbol{\mu}'_0$ (Algorithm 1)
$\boldsymbol{\mu}_{\text{opt}} \leftarrow \boldsymbol{\mu}'_0$
while $J(\boldsymbol{\mu}_{\text{opt}}) > \text{Err}_c$ **do**
  Find admissible solutions and corresponding regions $\mathcal{D}'$
  Sparse sampling in $\mathcal{D}'$
  Update *computational vademecum*
  Local minima and current global minimum $\boldsymbol{\mu}'_l$ (Algorithm 1)
  if $J(\boldsymbol{\mu}'_l)$ improves $J(\boldsymbol{\mu}_{\text{opt}})$ **then**
    Update the best, $\boldsymbol{\mu}_{\text{opt}} \leftarrow \boldsymbol{\mu}'_l$
  end
  $l \leftarrow l + 1$
end
Return $\boldsymbol{\mu}_{\text{opt}}$

5 Numerical examples

This section presents applications of the proposed strategy for welding identification problems. The reference is generated numerically and can be replaced by experimental measures in real cases. For simplification, the space-time *computational vademecum* with d controlled parameters is called d-D *computational vademecum*.

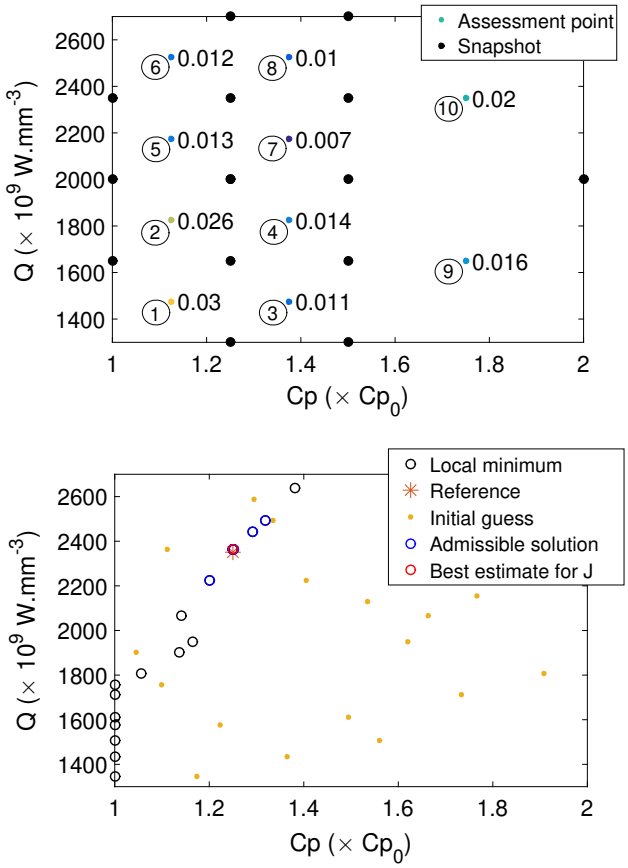

Fig. 13 Thermal parameter identification at iteration 1. Sampling grid with error assessment in design space (top) and multistart optimization (bottom)

5.1 2D thermal *computational vademecum*

In welding, temperature measures are usually employed to identify the thermal parameters of materials as well as the effective input power. Here an example of identifying two parameters is presented: thermal capacity C_p and effective input power Q, i.e. $\boldsymbol{\mu} = \left[C_p,\ Q\right]^T$, where C_p is varying from C_{p0} to $2C_{p0}$ with C_{p0} described in Fig. 10, Q is varying in [1300, 2700] $\times\ 10^9$ W.mm^{-3}. The evolution of temperature during welding is provided by 9 thermocouples located in three lines at different distances to loading. Figure 11 illustrates their positions on the workpiece.

The identification problem is then written as

$$\begin{cases} \text{Find} \quad \boldsymbol{\mu} \in \mathcal{D} \quad \text{s.t.} \\ \boldsymbol{\mu} = \underset{\boldsymbol{\mu}^* \in \mathcal{D}}{\arg\min}\ J\left(\boldsymbol{\theta}, \boldsymbol{\theta}^e, \boldsymbol{\mu}^*\right), \\ \text{with } J = \dfrac{\| \boldsymbol{\theta}(\mathbf{X}, t; \boldsymbol{\mu}^*) - \boldsymbol{\theta}^e(\mathbf{X}, t) \|_{\Omega_s \times \Omega_t}}{\| \boldsymbol{\theta}^e(\mathbf{X}, t) \|_{\Omega_s \times \Omega_t}}, \end{cases} \tag{30}$$

where the space-time norm $\| \bullet \|_{\Omega_s \times \Omega_t} = \sqrt{\sum_x \sum_t (\bullet)^2}$, the vector of parameters $\boldsymbol{\mu} = \left[C_p,\ Q\right]^T$ and the parameter domain $\mathcal{D} = [1,\ 2] \times [1300,\ 2700]$. The vector of quantity of interest reads

$$\boldsymbol{\theta}(\mathrm{p}, t) = \left[\theta(\mathrm{p}_1, t), \theta(\mathrm{p}_2, t), \ldots, \theta(\mathrm{p}_9, t)\right]^T. \tag{31}$$

And $\boldsymbol{\theta}^e$ designs the experimental reference.

Based on the proposed strategy, the space-time 2D *computational vademecum* is constructed by HOPGD with sparse grid sampling

$$\boldsymbol{\theta}(\mathrm{p}, t, C_p, Q) = \sum_{m=1}^{n} \boldsymbol{\Phi}^m(\mathrm{p}) \otimes \mathbf{V}^m(t) \otimes \boldsymbol{F}_1^m(C_p) \otimes \boldsymbol{F}_2^m(Q). \tag{32}$$

At the offline stage, the design space is sampled for a mean error of 3%. As shown in Fig. 12, five snapshots are selected in the parameter space. The center of each generated subdomain is chosen for error assessment. Then, multistart optimization with 20 different starting points are applied to find the global minima of current response surface. It is shown that admissible solutions are located in two subregions (1 and 2) and local refinements are needed to improve the prediction precision.

Subdomains 1 and 2 are explored at iteration 1. 9 snapshots are added in these regions. The new sampling grid and optimization results using the updated *computational vademecum* are depicted in Fig. 13. This iterative learning procedure is summarized in Table 3. The admissible solutions converge quickly to the reference values within two global iterations in the present case. Final identified values are [1.25, 2363], which are very close to the reference values [1.25, 2350]. Figure 14 confirms again the convergence of identification. The approximation of temperature evolution with identified parameters shows a good agreement with the "experimental" reference.

Table 3 Global iteration for thermal parameter identification

Iteration	Snapshots	Ref. C_p	Ref. Q	Iden. C_p	Iden. Q	J
0	5	1.25	2350	1.32	2444	0.0176
1	14	1.25	2350	1.25	2363	0.0048

Ref. denotes Reference values, Iden. denotes identified values

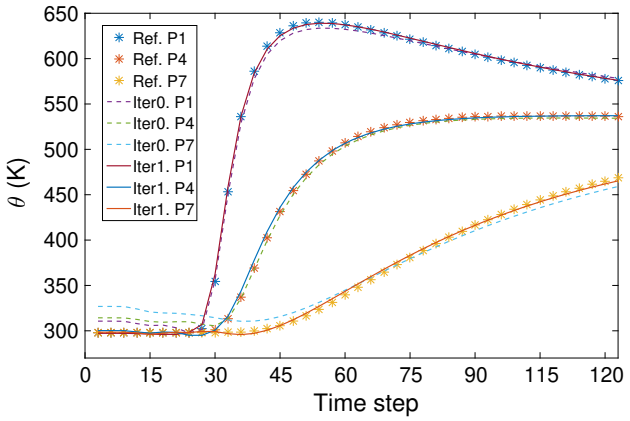

Fig. 14 Approximation with identified parameter values versus "experimental" reference

Table 4 Example of local optimization with SQP algorithm

Iteration	Function evaluation	J	Iden. C_p	Iden. Q
0	5	0.146555	1.66	2065
1	10	0.119662	–	–
2	15	0.066103	–	–
3	20	0.064368	–	–
4	25	0.024145	–	–
5	33	0.019985	–	–
6	38	0.016983	–	–
7 (conv.)	43	0.016937	1.14	2065

Table 5 Computational cost for thermal parameter identification

Iteration	Snapshots	Assessment points	Total simulations	Optim. time
0	5	4	9	2 min.
1	14	10	24	2 min.

Each FE simulation with 29571 elements and 7299 nodes takes ∽20 min

It should be noticed that each global step involves 20 local optimization problems in which objective function will be evaluated many times if numerical derivatives are not supplied. An example of local problem with initial guess at [1.66, 2065] is illustrated in Table 4. In this local problem, objective function is evaluated 43 times. This can be very prohibitive with standard identification approaches since 43 full simulations will be required in such case. When multistart methods are used, this easily becomes out of reach. The proposed method benefits from the real-time response of *computational vademecum*. Each local optimization can be performed within 10 seconds. The total cost for this identification is illustrated in Table 5. The total number of simulations remains small with respect to the online function evaluations, and increases only sightly with iteration number thanks to the online subspace learning strategy.

5.2 3D mechanical *computational vademecum*

The second example consists in the identification of three material constitutive parameters using residual stresses. The Young's modulus E, thermal expansion α and initial yield stress σ_y are supposed unknown and variant in $[0.5E_0, 1.5E_0] \times [0.5\alpha_0, 1.5\alpha_0] \times \left[0.5\sigma_{y0}, 1.5\sigma_{y0}\right]$ with the reference $E_0, \alpha_0, \sigma_{y0}$ described as Fig. 15. The 3D parametric domain is then $\mathcal{D} = [0.5, 1.5] \times [0.5, 1.5] \times [0.5, 1.5]$. Hence, the identification problem reads

$$\begin{cases} \text{Find} \quad \boldsymbol{\mu} \in \mathcal{D} \quad \text{s.t.} \\ \boldsymbol{\mu} = \underset{\boldsymbol{\mu}^* \in \mathcal{D}}{\arg\min}\, J\left(\sigma_{vm}, \sigma^e_{vm}, \boldsymbol{\mu}^*\right), \\ \text{with } J = \dfrac{\| \sigma_{vm}(\mathbf{X}; \boldsymbol{\mu}^*) - \sigma^e_{vm}(\mathbf{X}) \|_{\Omega_s}}{\| \sigma^e_{vm}(\mathbf{X}) \|_{\Omega_s}}, \end{cases} \tag{33}$$

where the vector of parameters $\boldsymbol{\mu} = \left[E, \alpha, \sigma_y\right]$. One supposes that all components of residual stresses are accessible by means of experiment. The quantity of interest used here is

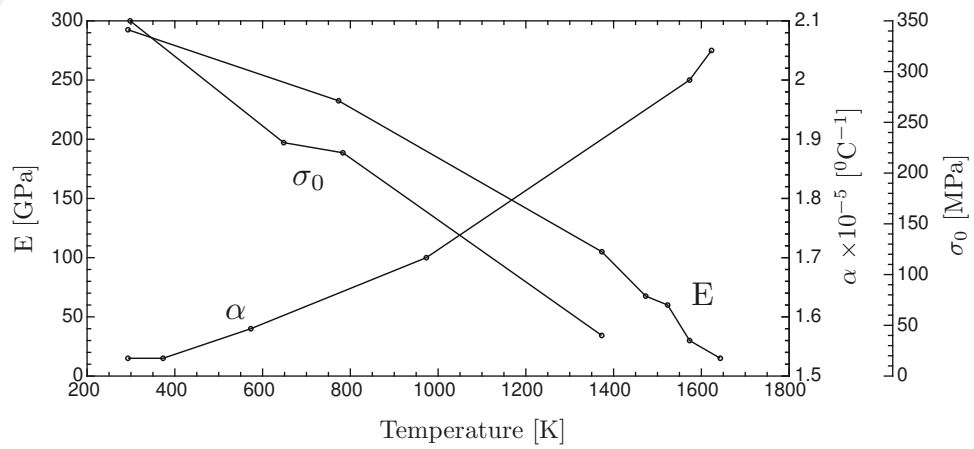

Fig. 15 Evolution of mechanical properties $(E_0, \alpha_0, \sigma_{y0})$ with temperature

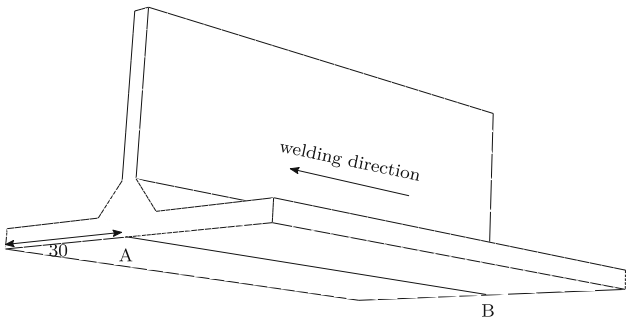

Fig. 16 Line of interest for residual stresses

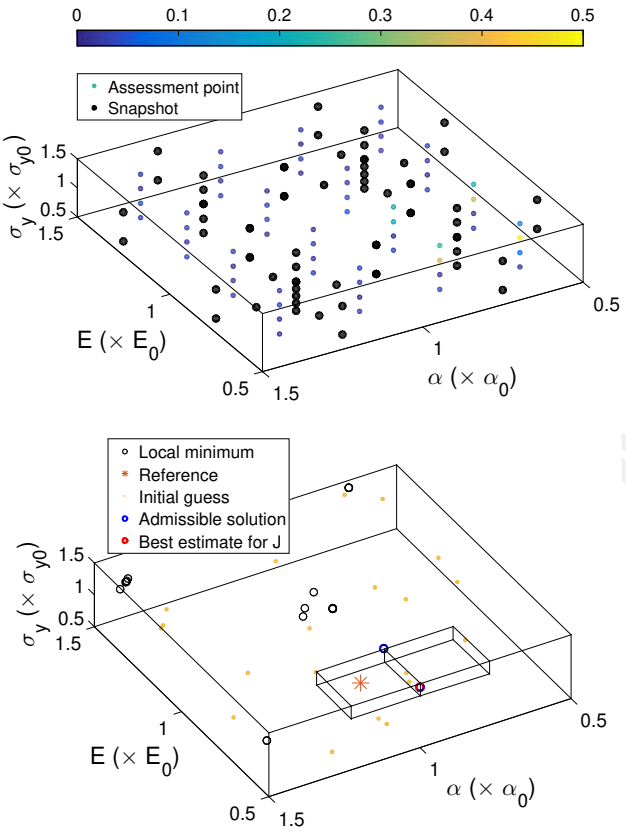

Fig. 17 Mechanical parameter identification at iteration 0. Sampling grid with error assessment in design space (top) and multistart optimization (bottom)

the equivalent residual stresses σ_{vm}, in particular, along the line AB as illustrated in Fig. 16.

The separated representation for the quantity of interest reads

$$\boldsymbol{\sigma_{vm}}(\mathbf{X}, t, E, \alpha, \sigma_y) = \sum_{m=1}^{n} \boldsymbol{\Phi}^m(\mathbf{X}) \otimes \mathbf{V}^m(t) \otimes \boldsymbol{F}_1^m(E) \otimes \boldsymbol{F}_2^m(\alpha) \otimes \boldsymbol{F}_3^m(\sigma_y). \quad (34)$$

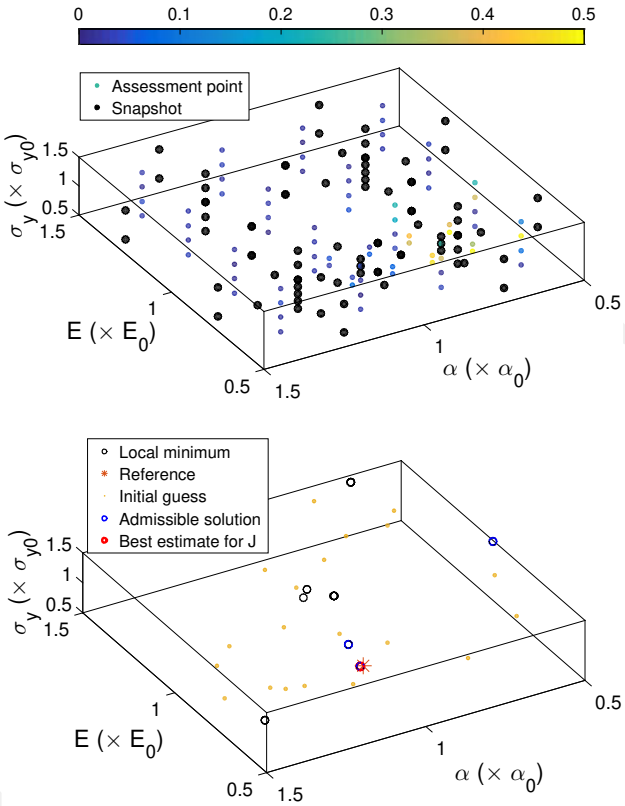

Fig. 18 Mechanical parameter identification at iteration 0. Sampling grid with error assessment in design space (top) and multistart optimization (bottom)

Figures 17 and 18 show the sampling grids and optimization results for the two first iterations. The initial grid containing 56 snapshots at step 0 is realized for an average approximation error of 5%. Two local regions are explored at step 1 according to the local minima provided by step 0. As shown in Table 6, the final identified values [0.625, 1.134, 1.377] for $[E, \alpha, \sigma_y]$ are very close to the reference [0.625, 1.125, 1.375]. It should be noticed that the critical relative error for J needs to be inferior to 0.01 for a high accurate identification. Figure 19 confirms that the residual stresses along the line AB are well reproduced with the identified parameters. Again, the computational cost increases slowly with iterations (see Table 7). The generation of snapshots and assessment points can be easily parallelized.

It should be highlighted that in this case, parameters are accurately identified without exploring precisely the whole design space. The proposed learning strategy can efficiently avoid redundant snapshots for problems with many local minima.

Table 6 Global iteration for mechanical parameter identification

Iteration	Snapshots	Ref. $[E, \alpha, \sigma_y]$	Iden. $[E, \alpha, \sigma_y]$	J
0	56	[0.625, 1.125, 1.375]	[0.500, 1.000, 1.450]	0.0236
1	69	[0.625, 1.125, 1.375]	[0.625, 1.134, 1.377]	0.0021

Ref. denotes Reference values, Iden. denotes Identified values

Table 7 Computational cost for mechanical parameter identification

Iteration	Snapshots	Assessment points	Total simulations	Optim. time
0	56	64	120	4 min.
1	69	80	149	4 min.

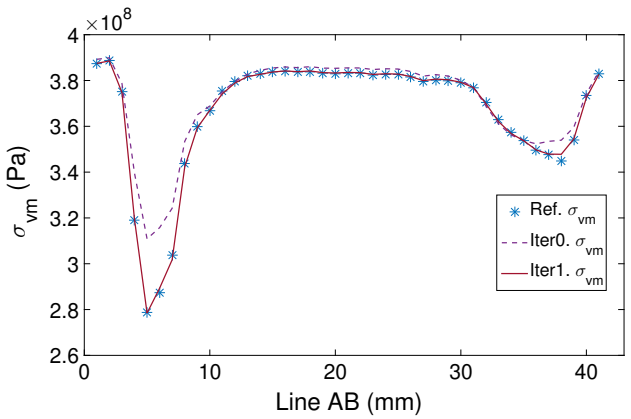

Fig. 19 Approximation of residual stresses with identified parameter values versus "experimental" reference

6 Conclusion

A datadriven framework for welding parameter identification has been proposed. The proposed method is based on *computational vademecum* that provides real time welding simulations. The welding *computational vademecum* is constructed using an *a posteriori* non-intrusive reduction method coupled with ABAQUS for generating the snapshots. The proposed online subspace learning allows updating the constructed *computational vademecum* with online uses. Furthermore, the global optimization method can efficiently detect the local minima and find the overall best solution. The identification examples using the proposed strategy have shown that the prediction of *computational vademecum* converges quickly to the optimal solution. The parameters values are accurately identified in both cases with very limited snapshots.

Further development can be carried out by considering the noise and uncertainties in experimental data. In that case, a stochastic approach should be used in the identification of parameters. Another improvement of the proposed method consists in the error indicator. The development of a residual based or a more mathematical error estimator can avoid the generation of data points for the error assessment.

Acknowledgements The authors gratefully acknowledge AREVA and SAFRAN for funding of this work within the framework of the "Life extension and manufacturing processes" teaching and research Chair.

References

1. Ammar A, Mokdad B, Chinesta F, Keunings R (2006) A new family of solvers for some classes of multidimensional partial differential equations encountered in kinetic theory modeling of complex fluids. J Non-Newton Fluid Mech 139(3):153–176
2. Amsallem D, Farhat C (2008) Interpolation method for adapting reduced-order models and application to aeroelasticity. AIAA J 46(7):1803–1813
3. Babkin A, Gladkov E (2016) Identification of welding parameters for quality welds in gmaw. Weld J 95(1):37S–46S
4. Barrault M, Maday Y, Nguyen NC, Patera AT (2004) An 'empirical interpolation'method: application to efficient reduced-basis discretization of partial differential equations. C R Math 339(9):667–672
5. Bessa M, Bostanabad R, Liu Z, Hu A, Apley DW, Brinson C, Chen W, Liu WK (2017) A framework for data-driven analysis of materials under uncertainty: countering the curse of dimensionality. Comput Methods Appl Mech Eng 320:633–667
6. Borzacchiello D, Aguado JV, Chinesta F (2017) Non-intrusive sparse subspace learning for parametrized problems. Arch Comput Methods Eng. https://doi.org/10.1007/s11831-017-9241-4
7. Bull AD (2011) Convergence rates of efficient global optimization algorithms. J Mach Learn Res 12(Oct):2879–2904
8. Canales D, Leygue A, Chinesta F, González D, Cueto E, Feulvarch E, Bergheau JM, Huerta A (2016) Vademecum-based gfem (v-gfem): optimal enrichment for transient problems. Int J Numer Methods Eng 108(9):971–989
9. Chaturantabut S, Sorensen DC (2010) Nonlinear model reduction via discrete empirical interpolation. SIAM J Sci Comput 32(5):2737–2764
10. Chinesta F, Ammar A, Cueto E (2010) Recent advances and new challenges in the use of the proper generalized decomposition for solving multidimensional models. Arch Comput Methods Eng 17(4):327–350
11. Chinesta F, Leygue A, Bordeu F, Aguado J, Cueto E, González D, Alfaro I, Ammar A, Huerta A (2013) Pgd-based computational vademecum for efficient design, optimization and control. Arch Comput Methods Eng 20(1):31–59
12. Cognard JY, Ladevèze P (1993) A large time increment approach for cyclic viscoplasticity. Int J Plast 9(2):141–157
13. Courard A, Néron D, Ladeveze P, Andolfatto P, Bergerot A (2013) Virtual charts for shape optimization of structures. In: 2nd ECCOMAS Young investigators conference (YIC 2013)

14. Ghnatios C, Masson F, Huerta A, Leygue A, Cueto E, Chinesta F (2012) Proper generalized decomposition based dynamic data-driven control of thermal processes. Comput Methods Appl Mech Eng 213:29–41
15. Goldak J, Chakravarti A, Bibby M (1984) A new finite element model for welding heat sources. Metall Trans B 15(2):299–305
16. González D, Alfaro I, Quesada C, Cueto E, Chinesta F (2015) Computational vademecums for the real-time simulation of haptic collision between nonlinear solids. Comput Methods Appl Mech Eng 283:210–223
17. González D, Masson F, Poulhaon F, Leygue A, Cueto E, Chinesta F (2012) Proper generalized decomposition based dynamic data driven inverse identification. Math Comput Simul 82(9):1677–1695
18. Holmes P, Lumley JL, Berkooz G (1998) Turbulence, coherent structures, dynamical systems and symmetry. Cambridge University Press, Cambridge
19. Hotelling H (1933) Analysis of a complex of statistical variables into principal components. J Educ Psychol 24(6):417
20. Ibañez R, Abisset-Chavanne E, Aguado JV, Gonzalez D, Cueto E, Chinesta F (2018) A manifold learning approach to data-driven computational elasticity and inelasticity. Arch Comput Methods Eng 25(1):47–57
21. Ibañez R, Borzacchiello D, Aguado JV, Abisset-Chavanne E, Cueto E, Ladeveze P, Chinesta F (2017) Data-driven non-linear elasticity: constitutive manifold construction and problem discretization. Comput Mech 60(5):813–826
22. Kerfriden P, Gosselet P, Adhikari S, Bordas SPA (2011) Bridging proper orthogonal decomposition methods and augmented newton-krylov algorithms: an adaptive model order reduction for highly nonlinear mechanical problems. Comput Methods Appl Mech Eng 200(5):850–866
23. Kirchdoerfer T, Ortiz M (2016) Data-driven computational mechanics. Comput Methods Appl Mech Eng 304:81–101
24. Kirchdoerfer T, Ortiz M (2018) Data-driven computing in dynamics. Int J Numer Methods Eng 113(11):1697–1710
25. Kolda TG, Bader BW (2009) Tensor decompositions and applications. SIAM Rev 51(3):455–500
26. Kolda TG, Lewis RM, Torczon V (2003) Optimization by direct search: new perspectives on some classical and modern methods. SIAM Rev 45(3):385–482
27. Leygue A, Coret M, Réthoré J, Stainier L, Verron E (2018) Data-based derivation of material response. Comput Methods Appl Mech Eng 331:184–196
28. Lu Y, Blal N, Gravouil A (2018) Adaptive sparse grid based hopgd: toward a nonintrusive strategy for constructing space-time welding computational vademecum. Int J Numer Methods Eng 114:1438–1461
29. Lu Y, Blal N, Gravouil A (2018) Multi-parametric space-time computational vademecum for parametric studies: application to real time welding simulations. Finite Elements Anal Des 139:62–72
30. Lu Y, Blal N, Gravouil A (2018) Space-time pod based computational vademecums for parametric studies: application to thermo-mechanical problems. Adv Model Simul Eng Sci 5(1):3
31. Maday Y, Patera AT, Turinici G (2002) A priori convergence theory for reduced-basis approximations of single-parameter elliptic partial differential equations. J Sci Comput 17(1–4):437–446
32. Martí R, Lozano JA, Mendiburu A, Hernando L (2016) Multi-start methods. In: Handbook of Heuristics. Springer, pp. 1–21
33. Meng L, Breitkopf P, Raghavan B, Mauvoisin G, Bartier O, Hernot X (2015) Identification of material properties using indentation test and shape manifold learning approach. Comput Methods Appl Mech Eng 297:239–257
34. Meng L, Raghavan B, Bartier O, Hernot X, Mauvoisin G, Breitkopf P (2017) An objective meta-modeling approach for indentation-based material characterization. Mech Mater 107:31–44
35. Modesto D, Zlotnik S, Huerta A (2015) Proper generalized decomposition for parameterized helmholtz problems in heterogeneous and unbounded domains: application to harbor agitation. Comput Methods Appl Mech Eng 295:127–149
36. Mosavi A, Rabczuk T, Varkonyi-Koczy AR (2017) Reviewing the novel machine learning tools for materials design. In: International conference on global research and education. Springer, pp 50–58
37. Muránsky O, Smith M, Bendeich P, Holden T, Luzin V, Martins R, Edwards L (2012) Comprehensive numerical analysis of a three-pass bead-in-slot weld and its critical validation using neutron and synchrotron diffraction residual stress measurements. Int J Solids Struct 49(9):1045–1062
38. Niroomandi S, Alfaro I, Cueto E, Chinesta F (2010) Model order reduction for hyperelastic materials. Int J Numer Methods Eng 81(9):1180–1206
39. Quesada C, González D, Alfaro I, Cueto E, Chinesta F (2016) Computational vademecums for real-time simulation of surgical cutting in haptic environments. Int J Numer Methods Eng 108(10):1230–1247
40. Rajan K (2015) Materials informatics: the materials "gene" and big data. Annu Rev Mater Res 45:153–169
41. Rozza G, Huynh DBP, Patera AT (2008) Reduced basis approximation and a posteriori error estimation for affinely parametrized elliptic coercive partial differential equations. Arch Comput Methods Eng 15(3):229–275
42. Ryckelynck D (2005) A priori hyperreduction method: an adaptive approach. J Computat Phys 202(1):346–366
43. Song J, Shanghvi J, Michaleris P (2004) Sensitivity analysis and optimization of thermo-elasto-plastic processes with applications to welding side heater design. Comput Methods Appl Mech Eng 193(42–44):4541–4566
44. Vitse M, Néron D, Boucard PA (2014) Virtual charts of solutions for parametrized nonlinear equations. Comput Mech 54(6):1529–1539
45. Zhang Y, Combescure A, Gravouil A (2015) Efficient hyper reduced-order model (hrom) for parametric studies of the 3d thermo-elasto-plastic calculation. Finite Elements Anal Des 102:37–51
46. Zhang Y, Combescure A, Gravouil A (2017) Efficient hyper-reduced-order model (hrom) for thermal analysis in the moving frame. Int J Numer Methods Eng 111(2):176–200